Planar heterojunction organic photovoltaic diodes via a novel stamp transfer process

2008 J. Phys.: Condens. Matter 20 475203

(http://iopscience.iop.org/0953-8984/20/47/475203)

J. Phys.: Condens. Matter **20** (2008) 475203 (8pp) doi:10.1088/0953-8984/20/47/475203

Planar heterojunction organic photovoltaic diodes via a novel stamp transfer process

Toby A M Ferenczi, Jenny Nelson, Colin Belton, Amy M Ballantyne, Mariano Campoy-Quiles, Felix M Braun and Donal D C Bradley

Department of Physics, Blackett Laboratory, Imperial College London, Prince Consort Road, London SW7 2BW, UK

E-mail: D.Bradley@imperial.ac.uk

Received 31 August 2008, in final form 7 October 2008
Published 29 October 2008
Online at stacks.iop.org/JPhysCM/20/475203

Abstract

Solution-processed, planar heterojunction organic photovoltaic diodes offer several potential advantages over bulk heterojunction structures in relation to electrode selectivity, reduced dark currents and suitability for fundamental studies. They have, however, received less interest in recent years, in large part due to fabrication difficulties encountered for sequential solution deposition steps. In this study, a novel stamp transfer technique that allows ready fabrication of planar heterojunctions from a variety of solution-processed organic materials is applied to construct bilayer heterojunctions from poly(3-hexylthiophene) (P3HT) and [6,6]-phenyl C_{61} butyric acid methyl ester (PCBM). We show that whilst 'as made' planar heterojunctions yield relatively poor photocurrent generation (compared to equivalent bulk heterojunction devices), thermal annealing improves their performance via creation of a diffuse mixed P3HT:PCBM interface layer. Good device performance with the anticipated low dark current is then achieved. Spectroscopic ellipsometry allows us to monitor the changes in the interface layer that result from annealing. We also model the external quantum efficiency spectra and show that they are consistent with the ellipsometry data. Furthermore, it is shown that good device performance is strongly dependent on the P3HT and PCBM layer ordering with respect to the electrodes, confirming the important role of electrode selectivity. Melting of 'incorrectly' ordered planar heterojunction devices (with donor next to the high work function and acceptor next to the low work function electrode) leads to the formation of bulk heterojunction devices, thereby recovering much of the desired performance.

1. Introduction

In recent years, significant improvement has been made in understanding and optimizing the performance of organic photovoltaic devices (OPVs) based on conjugated polymers. Their operation requires (i) photon absorption and exciton generation in a light-absorbing conjugated polymer (electron donor), (ii) exciton dissociation at an interface, usually with a second conjugated species (electron acceptor) and (iii) transport of the resulting charge carriers to and their collection at the appropriate electrodes. Optimization of the donor–acceptor structure should maximize the efficiency of each of these steps whilst preventing leakage of charge carriers through the 'wrong' electrode. An additional constraint is that the structure should be compatible with manufacture via low temperature, high throughput methods in order to retain the often cited low cost potential (in respect of both capital and energy expenditure) for organic photovoltaic devices.

The most successful donor–acceptor structure to date has been the bulk heterojunction [1–3], whereby both electron donating and accepting materials are deposited simultaneously as a mixed layer. Such a configuration creates a large and distributed donor–acceptor interface for exciton dissociation, which compensates for the limited exciton diffusion length in organic semiconductors and thereby leads to efficient

photocurrent generation and power conversion efficiencies (PCEs) of 4–5% [4–7]. The bulk heterojunction also meets the requirements for ease of processing since it can be processed as a single layer. However, it is hard to control formation of the interconnected pathways within each of the electron donor and acceptor materials required for efficient and selective charge carrier transport to the appropriate collection electrodes. Consequently, this structure may be associated with increased losses through charge carrier recombination and an increase in leakage currents relative to planar heterojunctions. This has led to the adoption of a multitude of different deposition protocols and post-deposition processing techniques to manipulate the blend micro-structure [8–13].

In contrast to bulk heterojunction device structures, planar bilayer heterojunctions have a smaller donor–acceptor interface area for exciton dissociation but they have better defined pathways for charge collection. Many such devices have been fabricated with either or both of the layers deposited using thermal evaporation, and PCE values of almost 3% have been reported [14–17]. Devices based on hybrid structures incorporating both planar heterojunctions and mixed layers can perform better and have displayed maximum conversion efficiencies in the region 4–5% [15, 16]. There have, in contrast, been relatively few reports of solution-processed planar heterojunction OPVs, a situation that may be attributed in large part to a lack of convenient deposition methods that avoid disruption of existing layers by each subsequent deposition. Such structures are nevertheless of keen interest due to their potential as high performance devices and as a test bed to further study organic–semiconductor physics, especially the nature and role of organic–organic interfaces.

Previously, solution-processed planar heterojunctions of conjugated polymers have been fabricated via the use of 'orthogonal' solvents for each layer [18], by ink-jet printing [19], by the use of a precursor route or cross-linkable material that can be rendered insoluble before solution depositing a second layer on top [20] or by an aqueous 'float-off' lamination technique [21]. Here, we use a recently reported stamp transfer technique [22] to create solution-processed planar heterojunctions. The principle of the method is to use a poly(dimethylsiloxane) (PDMS) stamp to transfer a solid organic film on top of an existing spin-coated layer. A detailed description of this method may be found elsewhere [22]. We note also that a related technique was recently reported, requiring however the use of a sacrificial, water soluble release layer during the transfer step [23].

In this paper, the stamp transfer method is applied to fabricate heterojunctions of poly(3-hexylthiophene) (P3HT) (as an electron donating material) and the fullerene derivative, [6,6]-phenyl C_{61}-butyric acid methyl ester (PCBM) (as electron acceptor). These materials were chosen principally because they have shown success in bulk heterojunction devices and their electronic and structural properties are well known. We note, however, that the stamp transfer technique described here is applicable to a much wider range of materials [22].

2. Experimental details

Baytron P, poly(3,4-ethylenedioxythiophene):poly(styrene-sulfonate) (PEDOT:PSS), from H.C. Starck GmbH, poly(3-hexylthiophene) (P3HT) (regioregularity 94.4%, molecular weight 26.0 kDa, polydispersity 2.0) from Merck Chemicals and [6,6]-phenyl C_{61} butyric acid methyl ester (PCBM) also from Merck Chemicals were used as received without further purification.

Chlorobenzene solutions comprising pristine materials P3HT (30 mg $m1^{-1}$) and PCBM (50 mg $m1^{-1}$) were prepared for planar heterojunction fabrication and blend solutions containing both P3HT (15 mg $m1^{-1}$) and PCBM (15 mg $m1^{-1}$) were prepared for bulk heterojunction fabrication. All solutions were spin-coated at 3000 rpm.

The PDMS stamps were prepared by casting a mixture of Sylgard 184 silicone elastomer (Dow Corning) and a curing agent (10:1 ratio Sylgard:curing agent by mass). The two components were stirred thoroughly in a beaker for 30 min and degassed in vacuo for an hour before being gently poured onto a 50 nm thickness Au-coated Si wafer, and cured at 70 °C in an oven overnight. The PDMS stamps were peeled away from the Au-coated silicon wafer after cooling, placed on a glass surface, and then cut into pieces (1.2×1.2 cm^2). The thickness of the PDMS was typically 4 mm. The resulting PDMS stamp structures were lifted with tweezers, attached to glass backing plates, and placed within a plasma asher (EMITECH K1050X) for surface treatment. The power was set to 30 W for 45 s and the working gas was air at 0.2 mbar pressure. Polymer layers were then spin-coated onto the PDMS immediately following plasma treatment.

Photovoltaic diode structures were fabricated via a combination of spin-coating and polymer transfer printing using pre-patterned indium tin oxide (ITO) coated glass substrates (1.2×1.2 cm^2 glass slides with an 0.8 mm wide ITO (25 Ω/square) stripe down the middle). The ITO coated glass substrates (PsiOTc Ltd, UK) were cleaned in an ultrasonic bath (30 min) using deionized (DI) water mixed with Decon 90 (20%), and subsequently rinsed three times with DI water, followed by sonication in pure DI water (30 min). They were finally dried using compressed air. PEDOT–PSS was then spin-coated (50 nm thickness) onto the patterned ITO/glass substrate and heated at 150 °C for 30 min. For planar heterojunctions the first semiconductor layer was spin-coated. The second semiconductor layer was then transfer printed according to the description given in [22]: glycerol was not, however, used to assist any of the transfer steps. Where a PCBM layer was transferred, no heat was applied at any point during the transfer process. Where a P3HT layer was transferred, the sample was heated to 130 °C on a hotplate for 20 s in order to achieve complete transfer.

Cathode stripes comprising Ca (10 nm) with an Al (100 nm) cap were sequentially deposited through a shadow mask using an Edwards 307A evaporator. The active photovoltaic diode area (defined by the overlap between orthogonal ITO and Ca/Al stripes) was 1.5 mm × 3 mm. After cathode deposition, the samples were transferred into a N_2 atmosphere glove box ($O_2 < 0.1$ ppm, $H_2O < 1$ ppm) for annealing and testing.

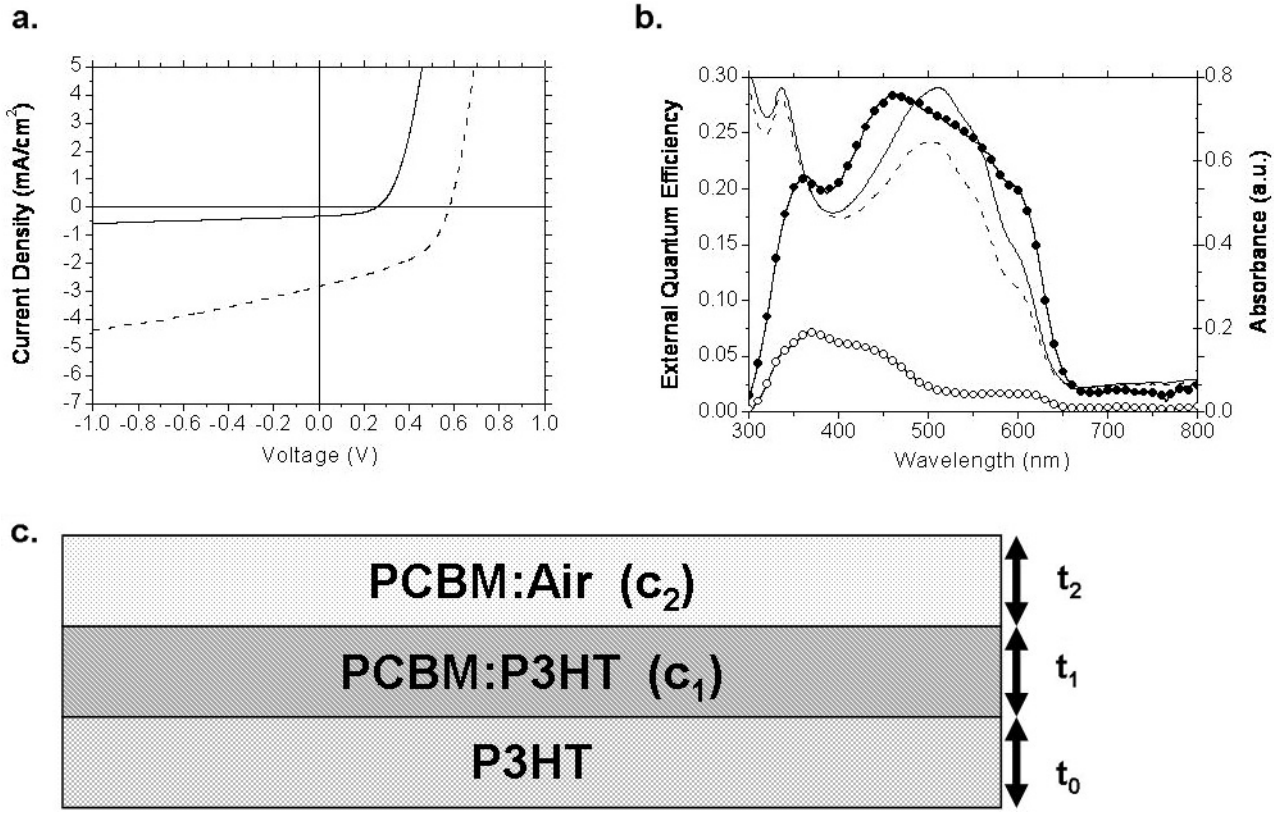

Figure 1. (a) Current density versus voltage characteristics under illumination for a typical P3HT/PCBM planar heterojunction device before (solid line) and after (dashed line) annealing. (b) External quantum efficiency (EQE) and absorption spectra before (EQE, empty circles; absorption, solid line) and after (EQE, filled circles; absorption, dashed line) annealing. (c) Schematic diagram of planar heterojunction model used in ellipsometric data fitting. The structure consists of a pristine P3HT layer with thickness t_0, a PCBM:P3HT blend layer with PCBM concentration c_1 and thickness t_1, a PCBM:air blend layer with PCBM concentration c_2 and thickness t_2.

Dark and photocurrent density versus voltage (J–V) characteristics were measured under simulated air mass 1.5 illumination at 1 Sun intensity using a Keithley 238 source measurement unit connected to a computer via a GPIB interface. The light source used was a 300 W xenon arc lamp solar simulator (Oriel Instruments) and the intensity was calibrated using a silicon photodiode pre-calibrated at the National Renewable Energy Laboratory (NREL), USA. For external quantum efficiency measurements, the monochromated (Bentham) output from a tungsten halogen source was used for illumination and the polymer photovoltaic diode response was calibrated using a Newport UV-818 photodiode.

Polymer films for absorption spectroscopy and ellipsometry were prepared as described above for photovoltaic diode fabrication but on cleaned Spectrosil B, quartz substrates (Kaypul Optics Ltd) rather than on PEDOT–PSS layers on patterned ITO coated glass substrates. Variable angle spectroscopic ellipsometry (VASE) was carried out using a SOPRA rotating polarizer (GESP 5) ellipsometer. Three incidence angles were recorded (close to the Brewster angle of each sample), with the wavelength scanned from 250 to 850 nm (5 nm steps). Analysis of the ellipsometry data of the pristine materials followed the standard critical point (SCP) model [24], with three and five peaks used to describe the dielectric functions of PCBM and P3HT, respectively. To fit the bilayers, a range of model structures was evaluated and the best was selected, based on the resulting standard deviation of the fit and the physical plausibility of the values produced. Absorption spectra were measured at normal incidence using a UV–visible spectrophotometer (V-560, Jasco).

3. Results and discussion

Figure 1(a) shows current density versus voltage characteristics under illumination before and after thermal treatment of a typical planar heterojunction device comprising glass/ITO/PEDOT:PSS/P3HT (∼60 nm)/PCBM (∼60 nm) /Ca/Al. It is evident that the untreated device performs poorly as a solar cell, with a low power conversion efficiency of ∼0.05%. This is due to both a small open circuit voltage and a small short circuit current. Upon heat treatment at 140 °C for 10 min in a dry nitrogen atmosphere (glove box), there is a significant improvement in both short circuit current and open circuit voltage leading to an increased power conversion efficiency of ∼1.6%. Previously, improvements in performance for bulk heterojunction devices upon thermal annealing have been attributed to several factors including increases in crystallinity leading to an enhanced absorption coefficient and higher charge carrier mobility, better formation of percolating pathways for more effective charge transport and collection,

and changes in vertical phase segregation promoting electrode selectivity [4–13, 25, 26]. The crystallinity of both P3HT and PCBM is inhibited when they are cast from solution in a mixed film such that the crystallinity of the blend is increased significantly upon heat treatment [25]. This does not happen in planar heterojunctions where each material is deposited separately, as is evident from the absorption spectra of figure 1(b), where the long wavelength shoulders indicative of P3HT crystallinity [4, 10] are already present in the unannealed film spectrum. Consequently, an increase in the absorption coefficient is unlikely to be able to explain the improved efficiency of the devices after annealing. Increases in charge carrier mobility in pristine P3HT and PCBM upon annealing may, in principle, contribute to the improvement in device performance upon annealing. However, whilst hole mobility enhancement has been observed through annealing in P3HT [27–29], these increases are not consistently found for the conditions employed here (10 min, 140 °C). Given the small thickness of the P3HT layer used here and the relatively high mobility of P3HT (even without annealing) and the low importance of mobility in bilayers (where charge recombination is reduced relative to bulk heterojunctions), we conclude that mobility enhancements are insufficient to explain the observed large improvement in photocurrent. In addition, no evidence for annealing-induced mobility enhancement has been found in pristine PCBM [30].

An alternative explanation for the improved performance upon annealing is that it arises from a modification of the organic–organic interface in the device. The glass transition temperatures of both P3HT and PCBM are in the region of 140 °C and it can be expected that annealing at this temperature leads to enhanced molecular mobility. In a blend, P3HT and PCBM tend to phase separate at 140 °C driven by the crystallization of each component. We suggest here that the initially abrupt interface between PCBM and P3HT becomes more diffuse during annealing driven by normal entropic principles. This proposal is supported by the results of spectroscopic ellipsometry measurements. Spectroscopic ellipsometry is a useful technique for determining layer structure within organic films and has previously been used to demonstrate vertical segregation in P3HT/PCBM bulk heterojunction films [25]. Ellipsometric scans were performed in the wavelength range 250–850 nm for three incidence angles. A number of model structures were evaluated with the goal of minimizing the standard deviation between model and data whilst using a limited number of free parameters. Examples of models evaluated include a pure bilayer and a bilayer with a P3HT:PCBM diffusion interlayer (Bruggemann mixing), with and without a PCBM layer on top. Comparison of the models was performed in terms of the standard deviation of the fits to the experimental ellipsometric data, as well as how physically meaningful the deduced parameters were. All of the models had a small and comparable number of fitting parameters (four to six). The model structure which we selected consists of a P3HT bottom layer covered by a mixed layer of PCBM and P3HT, with a mixed layer of PCBM and air (shown schematically in figure 1(c)). The mixed PCBM:air layer provides a useful way to factor in surface roughness and has been described elsewhere [26]. This model yielded low standard deviation fits with *both* the non-annealed and annealed structures (2.56×10^{-3} and 1.28×10^{-3} respectively). Care was also taken to check that the results give physically plausible values. In addition, the ellipsometry analysis was repeated for several independent samples to confirm the reliability of the results (our ellipsometry technique is discussed further in section 2).

Table 1. Parameters deduced from ellipsometry data for a simplified three level model of the planar heterojunction structures (cf figure 1(c)): layer thicknesses (t_0, t_1, and t_2) and mixed layer PCBM volume concentrations (c_1 and c_2) are given for both unannealed and annealed (10 min at 140 °C) devices. Errors given are estimated from the variation found between various model structures.

Parameter	Unannealed	Annealed
c_2 (%)	93 ± 2	80 ± 2
t_2 (nm)	41 ± 3	31 ± 3
c_1 (%)	91 ± 2	42 ± 2
t_1 (nm)	26 ± 3	61 ± 3
t_0 (nm)	63 ± 3	10 ± 3

Table 1 displays the results of fitting our ellipsometric data, namely the deduced thickness of each layer and the PCBM volume fraction within the two mixed layers. Before annealing, the P3HT layer thickness is found to be 63 nm. The mixed P3HT:PCBM and PCBM:air layers are both found to have high PCBM contents (>90%) and a combined thickness of 68 nm (since both these layers have similar compositions, their individual thicknesses are not significant). This fit is further supported by the good fitting (3.36×10^{-3}) of a simpler two layer P3HT/PCBM structure with thicknesses 65 nm/63 nm respectively. These results show that initially there is a well defined, essentially bilayer, planar heterojunction. The small amount of intermixing modelled within layer 2 (i.e. $1 - c_2 = 9 \pm 2\%$ P3HT content) is plausibly a simple result of the initial roughness of the P3HT layer that is readily seen in AFM images [27]. The layer thicknesses (t_0 and ($t_1 + t_2$)) found for the two layers are consistent with those expected from independent profilometry and ellipsometry measurements of pristine films spin-coated from solutions of the same concentration.

After annealing, the modelled thickness of the bottom P3HT layer decreases significantly, while the modelled P3HT content and thickness of the mixed P3HT:PCBM middle layer both increase. This supports the suggestion that inter-diffusion occurs at the interface. Given the small molecule nature of PCBM, it is likely that it is PCBM that drives this intermixing. We note that the modelled air content of the upper layer increases, indicating a slight increase in surface roughness. This may be due to crystal growth within the PCBM layer. We also note a decrease in the total film thickness. This may be due to an infilling by PCBM of voids observed in spin-coated P3HT films [17], which would also tend to enhance charge separation efficiency. A recent study of blends of P3HT and titanium dioxide [31] nanorods found that annealing led to an increase in photocurrent due to an improvement in interfacial contact. A similar effect may also contribute to the behaviour observed here for P3HT/PCBM.

Figure 1(b) shows the external quantum efficiency spectra of the planar heterojunction device before and after annealing. It is clear that there is a general increase in quantum efficiency upon annealing that is consistent with the improvement in device performance deduced from J–V measurements. In addition, the shape of the spectral response changes markedly. Before annealing, the wavelength contributing the most photocurrent is ∼360 nm, corresponding to photogeneration in the PCBM component, whereas after annealing the peak is closer to ∼450 nm, corresponding to photogeneration in the P3HT.

In an attempt to rationalize this behaviour, we use a simple model to estimate the external quantum efficiency spectrum from the known optical absorption properties of the materials and the layer thicknesses derived above. This consists in first calculating the fraction of the incident photon flux, A_{useful}, that is absorbed within regions of the active layers where photoinduced charge separation can occur. For blend regions with similar contents of donor and acceptor we assume that all absorbed photons lead to exciton dissociation. For pure layers of either component we assume that only photons absorbed within an exciton diffusion length (L_{P3HT} in the polymer and L_{PCBM} in the fullerene) of an interface with the other component lead to exciton dissociation. In computing A_{useful}, we use a transfer matrix method to calculate the electric field as a function of position within the layered structure for normally incident light. Each layer is discretized into 1 nm thick elements and the absorptance within each element is calculated from the gradient of the Poynting vector. The transfer matrix model is described elsewhere [32] and is similar to approaches used by other authors [33]. We then obtain the EQE by multiplying A_{useful} by a factor ϕ to account for losses due to interfacial recombination and light scattering, reflection and absorption in window layers. As input, the model requires the thicknesses of each layer (namely ITO (140 nm), PEDOT:PSS (70 nm), and the organic semiconductor layers (as obtained from ellipsometry)) and the complex refractive index as a function of wavelength for each material. The complex refractive index data for ITO, PEDOT:PSS and PCBM were taken from [34] and those for P3HT were obtained from spectroscopic ellipsometry [26]. The complex refractive index for the blend was obtained using a Bruggemann approximation. We vary ϕ, L_{P3HT} and L_{PCBM} to find the best fit of the model to the measured EQE for the non-annealed bilayer device, treating the two PCBM rich top layers as a single layer of pure PCBM of the appropriate thickness to conserve absorbance. Here, since the PCBM and P3HT absorb in different spectral regions, the comparison allows us to fit L_{P3HT} and L_{PCBM} independently once ϕ has been estimated. The layer thicknesses used are those obtained from spectroscopic ellipsometry as given in table 1. We then fit the model to the data for the annealed bilayer device using the layer thicknesses obtained via ellipsometry and the same values of ϕ, L_{P3HT} and L_{PCBM}. The annealed bilayer effectively determines the value of ϕ. From this fitting procedure, we obtain a value of 3 ± 1 nm for L_{P3HT}, 30 ± 10 nm for L_{PCBM} and 0.4 for ϕ. The exciton diffusion lengths are in reasonable agreement with values deduced from other experiments [35] and, although uncertainties remain, it is clear that L_{PCBM} is on the order of tens of nanometres and significantly larger than L_{P3HT}.

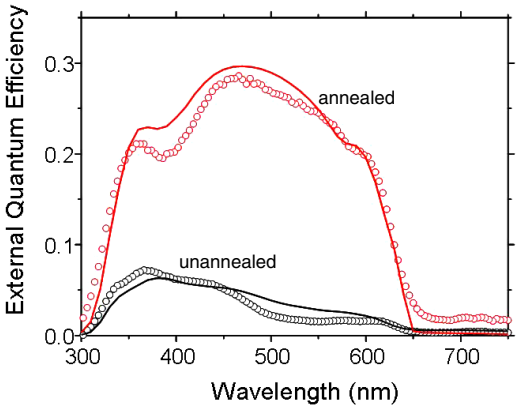

Figure 2. Measured device external quantum efficiency spectra (circles data) compared with theoretical spectra (solid lines) modelled for device structures identified by ellipsometry. The spectra shown are for devices with an unannealed planar heterojunction (black, lower EQE curves) and an annealed planar heterojunction (red (grey), upper EQE curves).

(This figure is in colour only in the electronic version)

The model results show good agreement with the experimental data (figure 2), giving basic confidence in the validity of the layer structure deduced by ellipsometric analysis and in the simple optical description of its photoresponse. The good agreement between data and model for both annealed and non-annealed structures supports the validity of the proposed structural changes deduced using ellipsometry. This therefore supports the explanation that the observed improvement in device performance is a result of intermixing at the interface between P3HT and PCBM. The analysis also shows that before annealing a significant fraction of the photocurrent arises from exciton generation in PCBM, since the EQE spectrum appears to be dominated by PCBM absorption. The modelling indicates that this is a direct consequence of the larger exciton diffusion length in PCBM than in P3HT. We note that the free parameters found here are described with the degree of precision deemed suitable given the available experimental data. This precision might be improved given more experimental data, such as those from EQE measurements of bilayers of varying layer thicknesses. Nevertheless, the obtained values do much to improve our understanding of this bilayer system. Given enough data, this technique might be used, in conjunction with a numerical fitting procedure, to independently estimate parameters such as the exciton diffusion length for new OPV materials.

The above analysis is supported by recent reports in the literature. Studies of copper phthalocyanine and buckminster fullerene (C_{60}) systems have shown that a structure intermediate between that of the bulk and planar heterojunctions, produced by incorporating three or more layers of varying donor–acceptor composition, similarly improves efficiency [15, 16]. In another study, planar heterojunctions composed of spin-coated P3HT and thermally evaporated C_{60} also showed a significant performance improvement upon annealing. Time-of-flight secondary ion

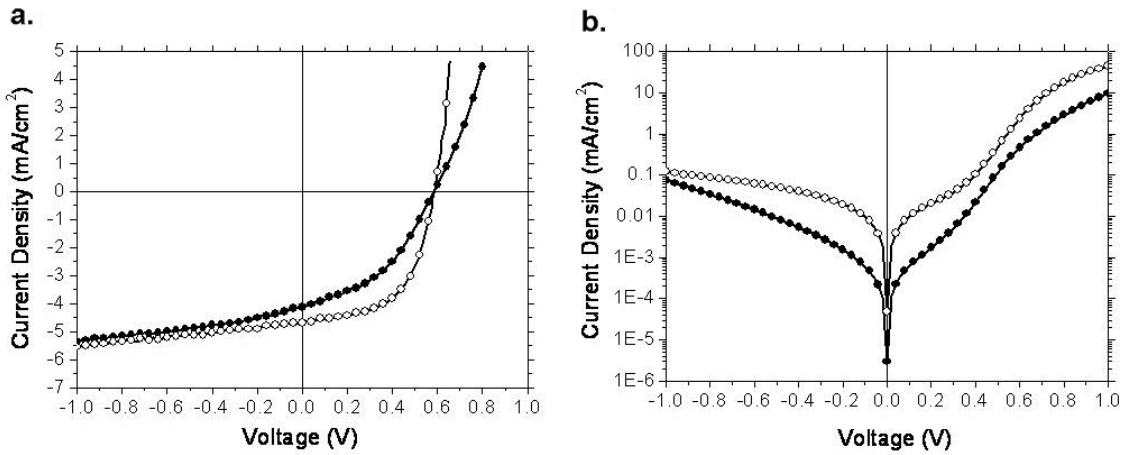

Figure 3. Current density versus voltage characteristics (a) under illumination and (b) in the dark for a P3HT:PCBM bulk heterojunction device (empty circles) (annealed 20 min at 140 °C) and a P3HT/PCBM planar heterojunction device (filled circles) (annealed 10 min at 140 °C).

mass spectroscopy (TOF-SIMS) for these latter structures confirmed that the organic–organic interface became broader and less distinct after annealing [17], just as deduced here.

Figures 3(a) and (b) show current–voltage characteristics under illumination and in the dark for an annealed device of the same layer structure and thicknesses as the device in figure 1 (but one with a higher short circuit photocurrent and power conversion efficiency). Also shown for comparison are the same data sets for a bulk heterojunction device with an active layer of similar total thickness to the bilayer (∼100 nm). It is clear that planar heterojunction devices can deliver short circuit current densities comparable with those for bulk heterojunction devices, although, at present, with a somewhat reduced fill factor. In addition, the planar heterojunction exhibits a significantly reduced dark current near $|V| = 0$. This may be attributed to the beneficial blocking effect of the pristine (un-mixed) layers near each electrode on leakage currents.

Figures 4(a) and (b) show current density–voltage and EQE characteristics for a planar heterojunction device with an 'inverted' bilayer structure, namely glass/ITO/PEDOT:PSS/PCBM (∼60 nm)/P3HT (∼60 nm)/Ca/Al. The order of the PCBM and P3HT layers will drive the photogenerated hole flux towards the low work function (Ca/Al) electrode and the corresponding electron flux towards the high work function (ITO/PEDOT:PSS) electrode, whilst the built in bias drives the fluxes in the opposite direction, such that both charge carrier types encounter large energetic steps at the electrodes. As a result, charge collection efficiency is expected to be reduced in relation to the 'correctly' ordered bilayer structure. In the device data shown here, this is confirmed by the significantly smaller short circuit current of the as fabricated 'inverted' structure (empty triangles) than that of the normal bilayer structure (see figure 1(a), solid line). However, after thermal annealing at 140 °C for 10 min (filled triangles), the performance of the inverse structure is remarkably improved with significant increases in both short circuit photocurrent and open circuit voltage. One possible explanation is that, in the case of the inverted bilayer, annealing leads to a substantial interpenetration of the layers, leaving a much higher probability for carriers to encounter percolating pathways leading to their correct collection electrodes. We suggest that annealing causes sufficient intermixing of the organic layers that charges dissociated at the organic–organic interface can be reasonably successfully transported via interpenetrating P3HT and PCBM networks and collected. It should be noted, however, that an alternative hypothesis has recently been proposed for an 'inverted' bilayer structure of pentacene and C_{60} [36]. It is proposed that the photocurrent in such a structure arises from exciton dissociation by charge transfer at each of the organic–electrode interfaces, with the excess electrons generated at one electrode and holes generated at the other electrode subsequently recombining at the organic–organic interface [36].

In order to improve the photocurrent generation from the P3HT component we have applied further heat treatments to the 'inverted' device. At 300 °C both P3HT and PCBM will be in a liquid-melt phase [25] and we can therefore expect that during a short period (10 s) of annealing at this temperature any crystalline regions will break up and large-scale intermixing will occur between the layers. The device can then be quenched rapidly to room temperature to produce a glassy blend active layer. The corresponding J–V characteristic is shown in figure 4(a) (empty circles). The poor performance of the device in this state is attributed to a reduction in the absorption coefficient due to the glassy nature (and correspondingly negligible crystallinity) of the active layer and to the lack of a developed interpenetrating network [25] with a suitable vertical segregation profile [26]. The observed J–V curve is entirely consistent with that of a typical 'melt-quenched' bulk heterojunction device [25].

If the quenched device is 're-annealed' at 140 °C (figure 4(a), filled circles), a substantially better performance is recovered. The much improved short circuit current (higher than that of the simply annealed 'inverted' planar heterojunction device) is in agreement with the effect of annealing on spin-coated bulk heterojunction films [4, 5, 25]. However, there is also an inflection, or 'kink', in the J–V curve, which has previously been related to inhibited charge

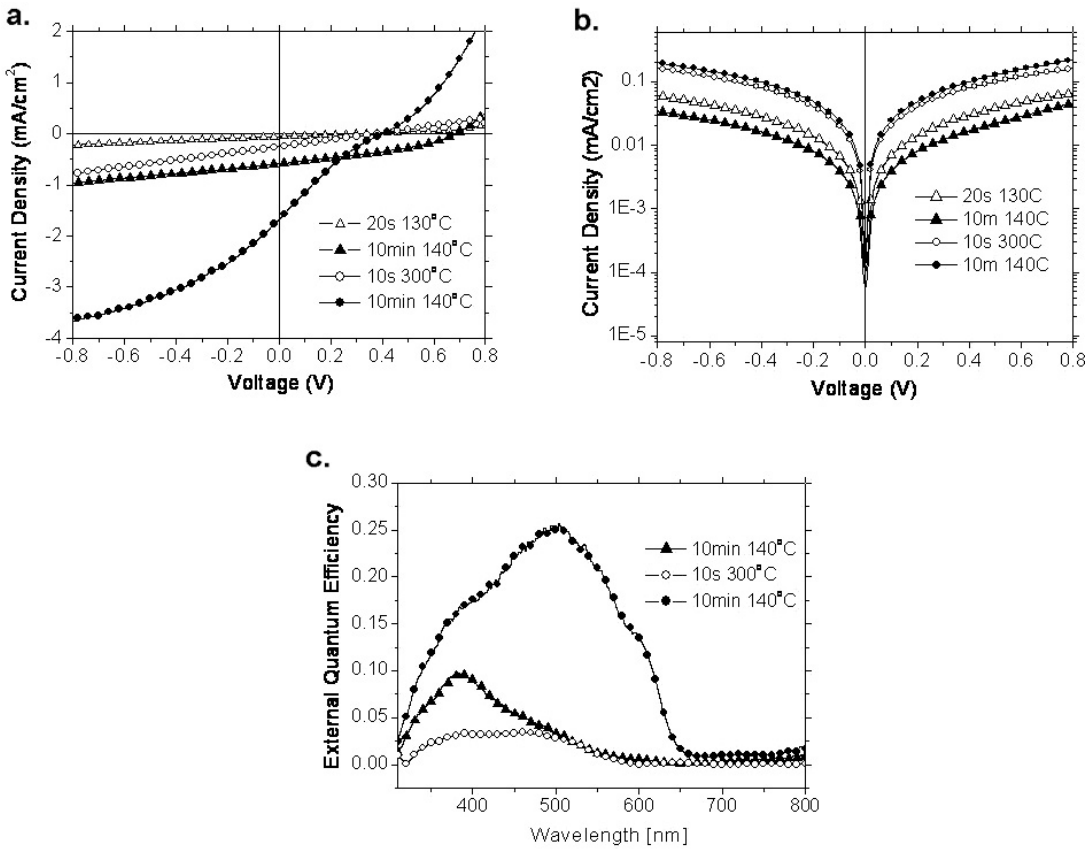

Figure 4. Current density versus voltage characteristics for an 'inverted' PCBM/P3HT planar heterojunction device subject to different thermal treatments (in sequence: 20 s at 130 °C, 10 min at 140 °C, 10 s at 300 °C and 10 min again at 140 °C). (a) Data under illumination; (b) data in the dark. (c) External quantum efficiency (EQE) spectra for the same device after 10 min at 140 °C (filled triangles), 10 s at 300 °C (empty circles) and a further 10 min at 140 °C (filled circles).

collection at the electrodes [37–39]. We believe that damage may occur to one or other of the electrodes during exposure to elevated temperatures at 300 °C. This proposal is supported by previous studies that show that the conductivity of PEDOT:PSS drops significantly after annealing at temperatures above 250 °C [40], and also by the lack of diode behaviour (with significant rectification) in the dark J–V after re-annealing (figure 4(b), filled circles), where an essentially symmetric characteristic is seen under forward and reverse bias. Judging by the photocurrent density at reverse bias (figure 4(a), filled circles), it is clear that the short circuit current would be considerably greater without this 'kink'. It is nevertheless evident that 'inverted' planar heterojunction structures may be heat treated into bulk heterojunction structures with a concomitant improvement in performance.

4. Conclusions

In conclusion, we have shown that the performance of as prepared planar heterojunction P3HT/PCBM photovoltaic diodes is driven to a large extent by absorption of photons in the PCBM. Improved performance is then dependent on void infilling and intermixing at the organic–organic interface through thermal annealing. Once sufficient intermixing between the layers has been achieved, the photocurrent of the planar heterojunction becomes comparable to that of an equivalent P3HT:PCBM bulk heterojunction device, but with the planar heterojunction structure exhibiting a significantly reduced dark current (advantageous for photodetector applications where dark current can set the limit of detection). Inverting the layer ordering of donor and acceptor materials results in reduced performance, but good performance can subsequently be recovered by melt processing, confirming the important role of electrode selectivity for optimum power conversion efficiency.

Acknowledgments

We thank the Royal Society Brian Mercer bequest, the UK Engineering and Physical Sciences Research Council (Doctoral Training Account and Basic Technology Programmes), the UK Department of Trade and Industry (Technology Programme) and BP Solar for financial support. We also thank Merck Chemicals Ltd for provision of P3HT and PCBM and Dr Lichun Chen for many helpful suggestions on stamp transfer printing.

Note added in proof. Two publications by Drees and co-workers have recently come to our attention. These papers study the effect of thermally annealing photovoltaic devices based on bilayers of C_{60} sublimed on top of spin-coated poly(2-methoxy-5-(2′-ethylhexyloxy)-1,4-phenylenevinylene) (MEH-PPV) [41] and poly(3-octylthiophene) (P3OT) [42]. In both cases evidence

was found for thermally induced inter-diffusion between the two layers leading to an up to one order of magnitude improvement in device performance. These earlier results provide additional support for the conclusions reached in the present study.

References

[1] Halls J J M, Walsh C A, Greenham N C, Marseglia E A, Friend R H, Moratti S C and Holmes A B 1995 *Nature* **376** 498

[2] Yu G, Gao J, Hummelen J C, Wudl F and Heeger A J 1995 *Science* **270** 1789

[3] Granström M, Petrisch K, Arias A C, Lux A, Andersson M R and Friend R H 1998 *Nature* **395** 257

[4] Kim Y, Cook S, Tuladhar S M, Choulis S A, Nelson J, Durrant J R, Bradley D D C, Giles M, McCulloch I, Ha C-S and Ree M 2006 *Nat. Mater.* **5** 197

[5] Li G, Shrotriya V, Huang J S, Yao Y, Moriarty T, Emery K and Yang Y 2005 *Nat. Mater.* **4** 864

[6] Xue J, Rand B P, Uchida S and Forrest S R 2005 *J. Appl. Phys.* **98** 124903

[7] Mihailetchi V D, Koster L J A, Blom P W M, Melzer C, de Boer B, van Duren J K L and Janssen R A J 2005 *Adv. Funct. Mater.* **15** 795

[8] Chirvase D, Parisi J, Hummelen J C and Dyakonov V 2004 *Nanotechnology* **15** 1317

[9] Inoue K, Ulbricht R, Madakasira P C, Sampson W M, Lee S, Gutierrez J, Ferraris J and Zakhidov A A 2004 *Proc. SPIE* **5520** 256

[10] Kim Y, Choulis S A, Nelson J, Bradley D D C, Cook S and Durrant J R 2005 *J. Mater. Sci.* **40** 1371
Kim Y, Choulis S A, Nelson J, Bradley D D C, Cook S and Durrant J R 2005 *Appl. Phys. Lett.* **86** 063502

[11] Moulé A J, Bonekamp J B and Meerholz K 2006 *J. Appl. Phys.* **100** 094503

[12] Ma W L, Yang C Y, Gong X, Lee K and Heeger A J 2005 *Adv. Funct. Mater.* **15** 1617

[13] Nguyen L H, Hoppe H, Erb T, Günes S, Gobsch G and Sariciftci N S 2007 *Adv. Funct. Mater.* **17** 1071

[14] Tang C W and Vanslyke S A 1987 *Appl. Phys. Lett.* **51** 913

[15] Heutz S, Sullivan P, Sanderson B M, Schultes S M and Jones T S 2004 *Sol. Energy Mater. Sol. Cells* **83** 229

[16] Yoo S, Domercq B and Kippelen B 2004 *Appl. Phys. Lett.* **85** 5427
Xue J G, Uchida S, Rand B P and Forrest S R 2004 *Appl. Phys. Lett.* **85** 5757

[17] Geiser A, Fan B, Benmansour H, Castro F, Heier J, Keller B, Mayerhoferc K E, Nuesch F and Hany R 2008 *Sol. Energy Mater. Sol. Cells* **92** 464

[18] O'Brien D, Weaver M S, Lidzey D G and Bradley D D C 1996 *Appl. Phys. Lett.* **69** 881

[19] Xia Y and Friend R H 2006 *Appl. Phys. Lett.* **88** 163508

[20] Burn P L, Grice A W, Tajbakhsh A, Bradley D D C and Thomas A C 1997 *Adv. Mater.* **9** 1171
Grice A W, Tajbakhsh A, Burn P L and Bradley D D C 1997 *Adv. Mater.* **9** 1174
Gather M C, Kohnen A, Falcou A, Becker H and Meerholz K 2007 *Adv. Funct. Mater.* **17** 191

[21] Ramsdale C M, Barker J A, Arias A C, MacKenzie J D, Friend R H and Greenham N C 2002 *J. Appl. Phys.* **92** 4266

[22] Chen L, Degenaar P and Bradley D D C 2008 *Adv. Mater.* **20** 1679

[23] Yim K H, Zheng Z, Liang Z, Friend R H, Huck W T S and Kim J-S 2008 *Adv. Funct. Mater.* **18** 1012

[24] Campoy-Quiles M, Heliotis G, Xia R, Ariu M, Pintani M, Etchegoin P G and Bradley D D C 2005 *Adv. Funct. Mater.* **15** 925
Campoy-Quiles M, Nelson J, Bradley D D C and Etchegoin P G 2007 *Phys. Rev.* B **76** 235206

[25] Mueller C, Ferenczi T A M, Frost J, Campoy-Quiles M, Bradley D D C, Smith P, Stingelin N and Nelson J 2008 *Adv. Mater.* **20** 3510

[26] Campoy-Quiles M, Ferenczi T A M, Agostinelli T, Etchegoin P G, Kim Y, Anthopoulos T, Stavrinou P N, Bradley D D C and Nelson J 2008 *Nat. Mater.* **7** 158

[27] Zen A, Pflaum J, Hirschmann S, Zhuang W, Jaiser F, Asawapirom U, Rabe J P, Scherf U and Neher D 2004 *Adv. Funct. Mater.* **14** 757

[28] Cho S, Lee K, Yuen J, Wang G, Moses D, Heeger A J, Surin M and Lazzaroni R 2006 *J. Appl. Phys.* **100** 114503

[29] Mattis B A, Chang P C and Subramanian V 2006 *Synth. Met.* **156** 1241

[30] Wobkenberg P H, Bradley D D C, Kronholm D, Hummelen J C, de Leeuw D M, Colle M and Anthopoulos T D 2008 *Synth. Met.* **158** 468
Warman J M, de Haas M P, Anthopoulos T D and de Leeuw D M 2006 *Adv. Mater.* **18** 2294

[31] Bouclé J, Chyla S, Shaffer M S P, Durrant J R, Bradley D D C and Nelson J 2008 *Adv. Funct. Mater.* **18** 22

[32] Felix B 2007 *PhD Thesis* University of London

[33] Pettersson L A A, Lucimara A, Roman S and Inganas O 2001 *J. Appl. Phys.* **89** 5564
Moulé A J, Bonekamp J B and Meerholz K 2006 *J. Appl. Phys.* **100** 094503

[34] Hoppe H, Sariciftci N S and Meissner D 2002 *Mol. Cryst. Liq. Cryst.* **385** 113

[35] Scully S R and McGehee M D 2006 *J. Appl. Phys.* **100** 034907
Luër L, Egelhaaf H J, Oelkrug D, Cerullo G, Lanzani G, Huisman B H and de Leeuw D 2004 *Org. Electron.* **5** 83
Kroeze J E, Savenije T J, Vermeulen M J M and Warman J M 2003 *J. Phys. Chem.* B **107** 7696
Peumans P, Yakimov A and Forrest S R 2003 *J. Appl. Phys.* **93** 3693

[36] Nanditha D M, Dissanayake M, Ross A, Hatton A, Curry R J and Silva S R P 2007 *Appl. Phys Lett.* **90** 113505

[37] Nelson J, Kirkpatrick J and Ravirajan P 2004 *Phys. Rev.* B **69** 035337

[38] Vogel M, Doka S, Breyer Ch, Lux-Steiner M Ch and Fostiropoulos K 2006 *Appl. Phys. Lett.* **89** 163501

[39] Glatthaar M, Riede M, Keegan N K, Sylvester-Hvid K, Zimmermann B, Niggemann M, Hinsch A and Gombert A 2007 *Sol. Energy Mater. Sol. Cells* **91** 390

[40] Huang J, Miller P F, Wilson J S, de Mello A J, de Mello J C and Bradley D D C 2005 *Adv. Funct. Mater.* **15** 290

[41] Drees M, Premaratne K, Graupner W, Heflin J R, Davis R M, Marciu D and Miller M 2002 *Appl. Phys. Lett.* **81** 4607

[42] Drees M, Davis R M and Heflin J R 2005 *J. Appl. Phys.* **97** 036103